Article

Vacuum Brazing Effect on the Interlayer Failure Behaviors of Elastic-Porous Sandwich Structure with Entangled Metallic Wire Mesh

Yuhan Wei, Ruixian Wu, Luming Zou, Niuniu Liu and Xin Xue *

School of Mechanical Engineering and Automation, Fuzhou University, Fuzhou 350116, China; n190220055@fzu.edu.cn (Y.W.); 200227141@fzu.edu.cn (R.W.); 200220083@fzu.edu.cn (L.Z.); nnliu@fzu.edu.cn (N.L.)
* Correspondence: xin@fzu.edu.cn; Tel.: +86-134-8908-5549

Abstract: Particular attention has been given to the complexity of the elastic-porous sandwich structure with entangled metallic wire mesh (EMWM), which is a novel rigid-flexible heterogeneous and symmetrical material. The orthogonal experiment design for vacuum brazing was adopted for sensitivity analysis of the key fabrication process on the performances of an EMWM sandwich structure. The shear behaviors of the sandwich structures with different vacuum brazing parameters (e.g., heating rate, brazing temperature, and holding time) were analyzed by mechanical experiments and an interfacial microstructure. The results indicated that the failure behavior of the sandwich structure could be divided into four stages in the mode-I experiment. In addition, the joint quality of the different vacuum brazing process could be shown by the mode-II experiment, and the failure behaviors involves three stages. Additionally, the failure behaviors of the sandwich structure were mainly associated with the deformation of the EMWM core and the strength of the brazing joint. In addition, the relationship between the joint strength and the shear performance of the sandwich structure was revealed through the interfacial microstructure. Furthermore, the importance of the optimized vacuum brazing parameters to fabricate the novel sandwich structure with the best joint performance was demonstrated in this work.

Keywords: elastic-porous sandwich structure; entangled metallic wire mesh; vacuum brazing; orthogonal experiment design; diffusion bonding behavior

1. Introduction

Sandwich structures have gained much attention due to their unique performances [1]. However, the traditional sandwich structures with the relatively rigid cores, such as honeycomb, form material, truss, and corrugation [2–8], have a limitation on their damping ability in vibration-reduction fields. The entangled metallic wire mesh (EMWM) is a complex and novel rigid-flexible heterogeneous material and shows excellent mechanical properties and high energy absorption [9,10]. In addition, Wang et al. [11] carried out compressive experiments to explore the difference between the sandwich structure with the metal rubber-filled corrugated hybrid core and the sandwich structure with the corrugated core. The results indicated that the sandwich structure showed better stiffness and energy absorption than the traditional corrugated sandwich structure. Furthermore, similar EMWM sandwich structures have already been applied for the vehicle braking system [12,13] and submarine foundation [14], as shown in Figure 1. Since the sandwich structure has a tricky problem regarding the delamination failure of the core/face-sheet interlayer, the reliable joint's quality plays a considerable role in the performance of the elastic-porous sandwich structure.
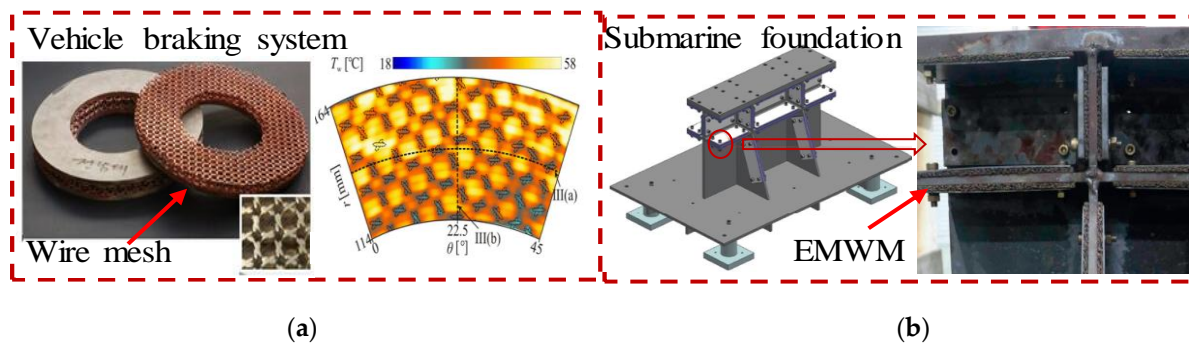
Figure 1. The engineering applications of EMWM sandwich structure: (**a**) vehicle brake disc; (**b**) submarine foundation.

Presently, there are some connection methods for the fabrication of sandwich structures, e.g., mechanical joining, gluing, and welding [15,16]. Traditionally, the mechanical connection involves a bolted connection, pining, and suturing [17–19]. However, the bolted connection section is susceptible to cracks. Furthermore, the performance of the sandwich structure is easily affected by the pining and stitch density. In addition, using these methods make it difficult to obtain a stable connection between the core and face because of there being few point joints or contacts. The connecting performance of the sandwich structure can be improved by the gluing method, to a certain extent. However, the application environment of the sandwich structure with adhesive can be limited by extreme conditions (e.g., humid environment and high temperature). In addition, Wang et al. [20] adopted shear experiments to test the effect of connection methods (gluing and vacuum brazing) on the EMWM sandwich structure. The results indicated that the shear performance of the sandwich structure by glued is lower than that of the brazed one. Therefore, the joint by vacuum brazing exhibited excellent joint strength. The welding methods mainly included laser-welding, induction welding, liquid diffusion welding, and vacuum brazing [21]. The oxidation of internal wires can be avoided by vacuum brazing, which can affect the EMWM performance. In addition, there are some advantages of the vacuum brazing technology, such as the simple operation, cost-effectiveness, and high joint strength [22]. However, a proper vacuum brazing parameter is vital to obtain an excellent mechanical performance of the brazing joint [23].

Many studies have attempted to achieve the excellent joint performances of sandwich structures. For example, the shear performance of the brazed joint has a positive relationship with the brazing temperature and holding time by Chen et al. [24]. Liu et al. [25] studied the effect of brazing temperature and time on the joint performance of a TC4 alloy. The results indicated that the brazing time and temperature are closely related to the microstructure and shear performance of the brazed joint. In addition, the shear strength of the joint positively correlates with the brazing time, which first increases and then decreases along with the increasing brazing temperature. In addition, different brazing parameters have a dramatic effect on the joint's interfacial microstructure. Zaharinie et al. [26] found that the brazing temperature can affect the diffusion of the constituents between the based material and the solder to affect the joint performance. Moreover, the brazing joint interlayer is stated to form granulated and crack when the brazing temperature is too high. Chakraborty et al. [27] compared the effect of different brazing temperatures on the microstructure, along with the hardness, and found that the volume fraction of the precipitates and the interface hardness in the joint section decreased with the increase in the brazing temperature. Jiang et al. [28,29] analyzed the influence of different holding times on tensile strength and the microstructure of a plate-fin structure. It was revealed that the structures' tensile strength first increased and then decreased by increasing the brazing time. The brazing time has an obvious effect on the brittle boride components. They also proposed a new cooling method to improve the joint performance. The results exhibited

that thermal cracks in the joint section could be created by a quick cooling method that can make the joint strength decrease.

The outline of this work can be drawn as follows. First, the whole fabrication technology of the elastic-porous sandwich structure is introduced, as well as the orthogonal experiment design for the sensitivity analysis of key parameters. Second, the influence of the vacuum brazing process on the failure behavior of the elastic-porous sandwich structure is addressed. Third, the effect of the vacuum brazing parameter on the interlayer microstructure is performed. Finally, the role of the vacuum brazing parameter on the shear performance of the sandwich structure is analyzed and discussed.

2. Materials and Methods

2.1. Materials

2.1.1. GH4169

The GH4169 superalloy is an age-hardening Ni-Fe-Ni alloy, which is also termed Inconel 718, and the chemical compositions are shown in Table 1. It exhibits excellent characteristics of creep resistance, antioxidant, and anti-fatigue. Additionally, it has a superior advantage over other Nickel-based alloys owing to the content of the Nb element [30]. Therefore, the GH4169 panel, which had a thickness of 0.8 mm, was adopted as the facesheet in the sandwich structure.

Table 1. Chemical compositions of the GH4169 superalloy.

Element	Si	Co	Cr	B	Nb	C	Al	Ni	Fe
Wt. %	0.13	0.03	17.72	0.02	5.11	0.042	0.55	51.83	Bal.

2.1.2. Solder

The BNi-2 and the base metal (GH4169) are the Nickel-based alloys, and the working temperature of brazing joint by BNi-2 can tolerate more than 1000 °C. Thus, foil material of BNi-2 was adopted as a solder in this study, and the chemical compositions are shown in Table 2. In addition, the optimization brazing temperature of BNi-2 is 1010~1177 °C. The solidus and liquidus temperatures of the BNi-2 are 970 °C and 1000 °C, respectively.

Table 2. Chemical compositions of the BNi-2.

Element	Si	Co	Cr	B	Fe	C	p	Ni
Wt. %	4–5	0.1	6–8	2.75–3.5	2.5–3.5	0.06	0.02	Bal.

2.1.3. EMWM Core

Belonging to a unique class of the elastic-porous materials, the EMWM provides additional advantages (such as resistance of the high/low temperature and corrosion to prolong service life) except for damping vibration, as against traditional rubber. Furthermore, the different wire material was also developed to manufacture EMWM, e.g., stainless steel [31], hybrid materials [32,33], shape memory [34], and Nickel-based [35]. Due to the excellent characteristics of creep resistance, antioxidant, and anti-fatigue, the GH4169 wire material was adopted in the work to meet the environmental adaptability, such as high-temperature resistance. The excellent mechanical performance of the EMWM core relies on its fabrication technology, and the internal structure is composed of complex, arranged, and entangled helix wires, as shown in Figure 2. There are several microscopic deformation modes such as friction, slipping, and extrusion among the internal wires when the EMWM is subjected to a complex load. Furthermore, it can play a massive impact on the damping vibration.
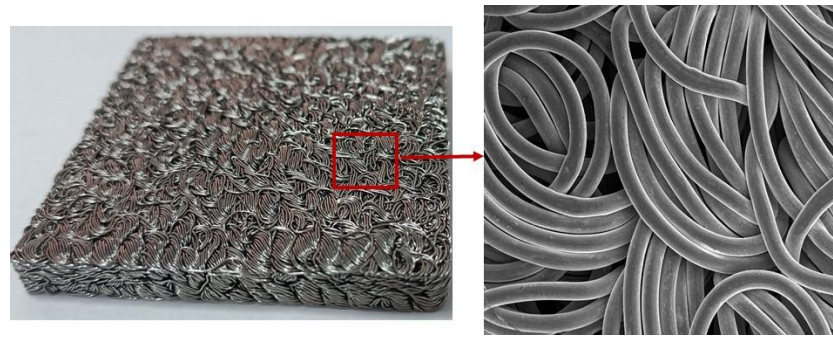
Figure 2. Microscopic characteristic of the EMWM core.

2.2. Fabrication of EMWM Core

There are four steps involved during the fabrication of the EMWM [36], as shown in Figure 3. The first step is the selection of the wire material (e.g., the metal wire type and wire diameter) according to different applied environments. In this work, EMWM was fabricated by GH4169 wires with diameter of 0.3 mm. The second step is twisting of the selected metal wire into spiral coil with the diameter of 3 mm by using in-house winding machine. The third step mainly involves drawing the spiral coil and entangling wire mesh by using in-house numerical control device to obtain an entangled blank. The last step is compressive formation. The relative density (ρ) of EMWM is given as follows:

$$\rho = m/(l \times w \times t), \tag{1}$$
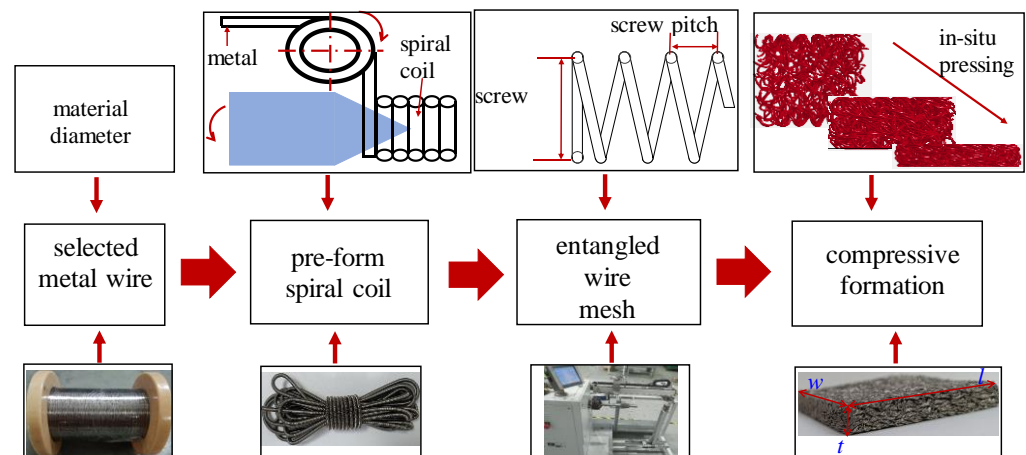
Figure 3. Fabrication technology of EMWM core.

The ρ is relevant to the dimensions of EMWM material (l, w, t) and the mass of GH4169 wires (m), as shown in Equation (1). In this work, the dimensions of EMWM are $50 \times 60 \times 7$ mm and the relative density (ρ) is 2.5 g/cm^3.

2.3. Fabrication Technology of Elastic-Porous Sandwich Structure

In this study, the GH4169 materials are used for the upper/lower face-sheet. The elastic-porous sandwich structure is fabricated using vacuum brazing. There are three steps involved in the fabrication technology of the sandwich structure, which are as follows: First, the GH4169 face-sheet, EMWM, and the fixture are assembled, as shown in Figure 4a. Second, the pre-brazing part is put into the vacuum furnace, which is operated as per the operating procedure of the required brazing heating process. The vacuum furnace (GSL-1400X, Hefei Kejing Material Technology Company, Hefei, China) with a maximum temperature of 1400 °C was adopted in the work. The vacuum atmosphere of the furnace is maintained below 2.5×10^{-3} Pa by operating the vacuum system. It is worth noting that the

vacuum system works during the vacuum brazing to ensure that the furnace atmosphere is kept to avoid sandwich structure oxidation. The heating curve [Figure 4c] relies on the vacuum brazing parameters (e.g., heating rate, brazing temperature, and holding time). Furnace cooling was selected in this study. Third, the elastic-porous sandwich structure moves when the furnace is at room temperature (20 °C), as shown in Figure 4d. The parameters of the EMWM sandwich structure are shown in Table 3.
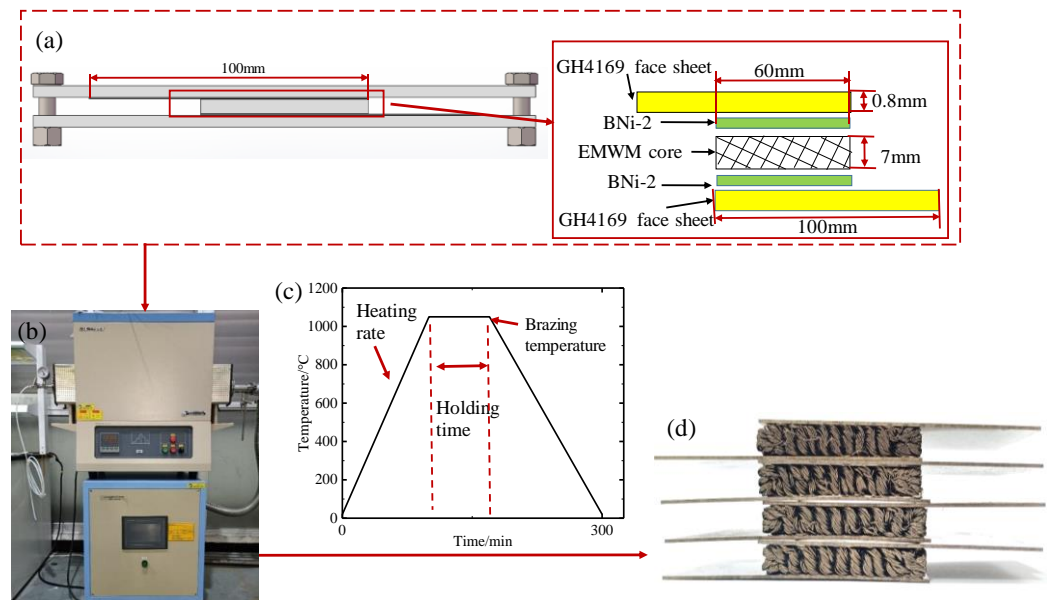
Figure 4. Vacuum brazing technology of the elastic-porous sandwich structure: (**a**) assembly of the sandwich structure, (**b**) vacuum furnace, (**c**) heating process, (**d**) EMWM sandwich structure.

Table 3. The parameter of the EMWM sandwich structure.

Face-Sheet		Width (mm)	EMWM Core		
Length (mm)	Thickness (mm)		Length (mm)	Thickness (mm)	Density (g/cm^3)
100	0.8	50	60	7	2.5

3. Experiments

3.1. Orthogonal Experiment Design

The orthogonal experiment design (OED) [37,38] was used to study the effect of vacuum brazing technology, and the OED L_9 (3^3) was arranged based on the fabrication parameters of the vacuum brazing process. According to the vacuum brazing process, three factors (e.g., heating rate, brazing temperature, and holding time) were selected, each with three different levels, as listed in Table 4. The brazing temperature is decided by the liquidus temperature of the solder and the solidus of the based metal. Thus, according to the solidus and liquidus temperatures of BNi-2 and GH4169, the selected brazing temperature is 1010~1090 °C in this work.

Table 4. The levels and factors affecting the vacuum brazing.

Levels	Factors		
	A: Brazing Temperature (°C)	B: Heating Rate (°C/min)	C: Holding Time (min)
1	1010	4	10
2	1050	7	20
3	1090	10	30

3.2. Simple Shear Experiments

The distribution of shear load on a sandwich structure is relative to the joint strength between the core and face-sheet [1–5]. In this work, two shear experiments (mode I and mode II) were performed to study the relationship between the shear performance of the elastic-porous sandwich structure and the vacuum brazing parameters. The responses of the elastic-porous sandwich structure on mode-I experiments were measured using a universal testing machine (WDW-T200, China Jinan Tianchen Machine Manufacture company, Jinan, China), which had a maximum force capacity of 100 kN, as shown in Figure 5. In addition, according to the ASTM C273-00 standard, the shear experiments were carried out under the displacement rate of 1 mm/min. To ensure the credibility of the conclusions, three replicate experiments were conducted for the sandwich structure at room temperature, which was fabricated by the same brazing process. The equivalent shear modulus (G_{eq}) of the elastic-porous sandwich structure can be calculated by the following equation:

$$\tau = F/(w * l), \tag{2}$$

$$\gamma = \Delta l / t_1 \tag{3}$$

$$G_{eq} = \tau / \gamma = F * t_1 / (\Delta l * l * w), \tag{4}$$
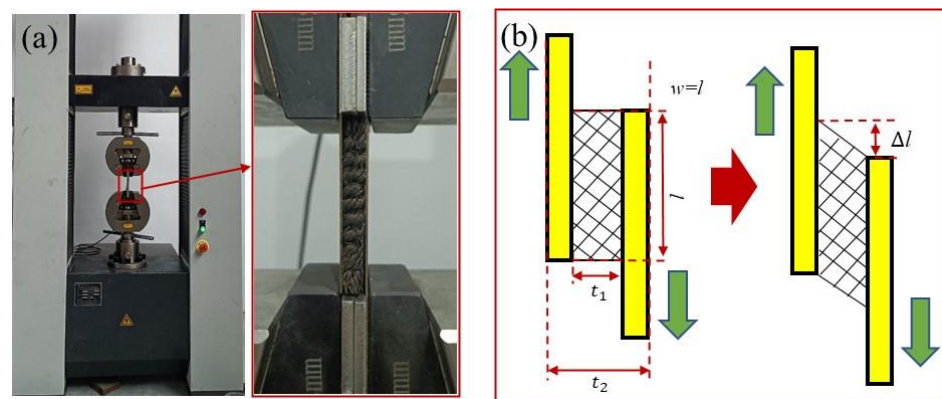
Figure 5. Mode-I experiment: (**a**) overview of the universal testing machine, (**b**) schematic of the specimen during the experiment.

As shown in Figure 6a, the specimens were fabricated to analyze the joint strength using a different vacuum brazing process. The three-helix wires and the face-sheet were fabricated by using the same vacuum brazing process with the sandwich structure. As shown in Figure 3, these equidistant coils with a screw pitch of 3 mm were obtained by drawing the helix wire. The mode-II experiments were also carried out at room temperature by a SHMADZU universal testing machine (AG-X plus, Japan), and more than three specimens were tested for the same brazing parameters. In addition, the displacement-control mode was adopted, and the application of the displacement rate was 1 mm/min.

In order to analyze the joint quality by different vacuum brazing processes, the macro and microstructure of the specimens can be characterized by a scanning electron microscope (SEM, Nova NanoSEM 230, FEI Company, Hillsboro, OH, USA). Wire cutting and filling epoxy resin were adopted to fabricate some samples. Moreover, a series of operating processes, involving ground, polishing, cleaning, and drying, was used to fabricate samples, which are exhibited in Figure 7. In addition, Figure 7 exhibits the typical microstructure characterization of the vacuum brazing joint interface in the EMWM sandwich structure.

Figure 6. Mode-II experiment: (**a**) the specimen, (**b**) experiment setup.

3.3. Microstructure Characterization
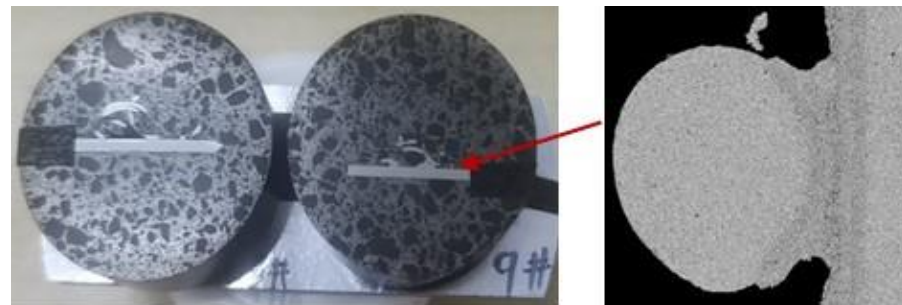
Figure 7. Typical microstructure characterization of the vacuum brazing joint.

4. Results and Discussion

4.1. Typical Failure Behaviors of the EMEM Sandwich Structure under Mode-I Experiment

Figure 8 shows the typical failure behavior of the EMWM sandwich structure under the mode-I experiment. According to the curve and failure behavior, there are four stages for the EMWM sandwich structure in the mode-I shear experiment, e.g., linear, gradual-soft deformation, damage deformation, and stable damage failure. Four different modes exhibit the failure deformation of the elastic-porous sandwich structure, as shown in Figure 8. The first stage is the linear stage, which is a small deformation stage. During this stage, the sliding between the helix wires of the EMWM is non-significant and the wires are in the elastic stage. Therefore, the deformation of helix wires shows elastic deformation. In addition, there is no obvious characteristic change in the EMWM sandwich structure, and the equation of G_{eq} is effective in this stage. With displacement increasing, the relative movement increases among the helix wires. Thus, slight delamination was shown in the EMWM core. However, this damage is irreversible for the EMWM core. Therefore, the trend of non-linearity began to be exhibited at this period, as well as the failure behavior of the sandwich structure. Additionally, the gradual-soft performance of the EMWM material was beginning to present in the second stage. Subsequently, when an obvious dislocation appears between the two face-sheets and the force, the failure behavior of the EMWM sandwich structure is in the third stage. The internal wires of the EMWM core were constantly straightened and peeled from the entangled static by constantly loading. Furthermore, obvious deformation appeared in the EMWM core, and the resistance ability of the EMWM exhibited a fast decrease trend. Finally, the IV stage of the sandwich structure presents a soft feature. The helix wires are not a complete failure because of the special performance and characteristics of the EMWM material. In this stage, the sandwich structure exhibits a certain bearing capacity. Therefore, the elastic-porous sandwich structure could still have the ability to bear the shear load. It is worth noting that the helix wires cannot be completely peeled from the face-sheet within a short period.
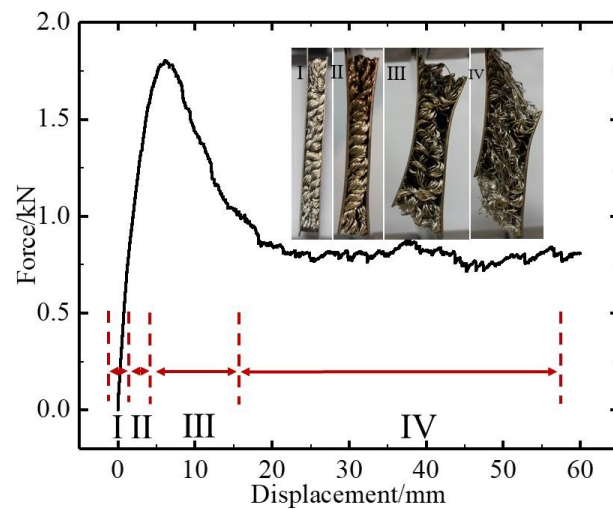
Figure 8. The typical failure behaviors of the sandwich structure under mode-I experiment.

Figure 8 shows the little helix wires of the EMWM peeling from the face-sheet and fracture. However, these conditions were straightened and snapped during stage IV. Noticeable scratches occurred on the sandwich structure after the shear experiment, as shown in Figure 9. As shown in Figure 9, there are two forms of the metallic wires in the core, which include helix wires and straightened wires. The EMWM core is subjected to the pull-shear force during the shear process. The middle metallic wires of the core gradually lost their entangled state and snapped when the wires were pulled up to a certain extent. Furthermore, due to the interaction movement of the wires, dry friction deformation and certain damage occurred. However, the helix wires, which were in the brazing joint area or near the face-sheet, almost retained their original shape. Furthermore, only a few wires had peeled from the face-sheet. In summary, the failure behaviors of the elastic-porous sandwich structure involve three behaviors, e.g., the delamination failure of the EMWM core, internal friction damage of the helix wires, and peeling failure.
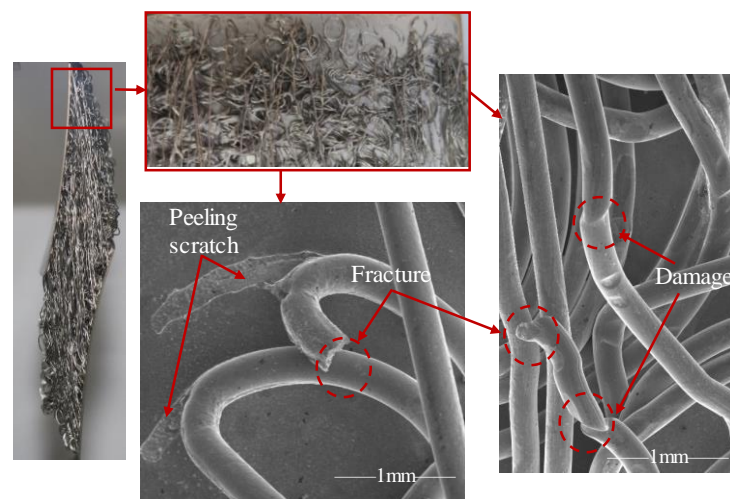
Figure 9. Characteristic of the sandwich structure after mode-I experiment.

4.2. Effect of Vacuum Brazing Parameter on Shear Properties of the EMEM Sandwich Structure

The specimens with different vacuum brazing processes listed in Table 5, were fabricated and tested to analyze the effect of the vacuum brazing process on the shear properties of the sandwich structure. The evaluations of the shear performance were selected and obtained through the force–displacement curve on the shear experiment. In addition,

the average value was obtained from the three repetitive experiments, and the G_{eq} of the sandwich structure was calculated by Equations (2)–(4).

Table 5. Shear properties' evaluations of the sandwich structure in OED L$_9$ (3^3).

Trial No.	Factors			Evaluations		
	A (Brazing Temperature (°C))	B (Heating Rate (°C/min))	C (Holding Time (min))	Maximum Force (kN)	Energy Absorption (J)	G_{eq} (MPa)
S1	1 (1010)	1 (4)	1 (10)	1.88	50.18	12.9
S2	1	2 (7)	2 (20)	1.60	35.05	12.5
S3	1	3 (10)	3 (30)	1.44	42.85	8.4
S4	2 (1050)	1	2	1.53	50.52	12.7
S5	2	2	3	1.81	56.61	12.0
S6	2	3	1	1.50	41.72	8.0
S7	3 (1090)	1	3	2.01	62.38	13.3
S8	3	2	1	1.89	58.18	10.9
S9	3	3	2	2.39	72.02	13.7

The changing trend of the selected three evaluations (maximum force, energy absorption, and G_{eq}) in the prepared nine specimens are shown in Table 5 and Figure 10. The value of S9 is maximum, and the value of S3 is minimum. In addition, it is shown that different vacuum brazing processes can affect the shear performance of the sandwich structure. Moreover, the three selected evaluations for the shear performance of the elastic-porous sandwich structure exhibit a similar changing trend, as shown in Figure 10.
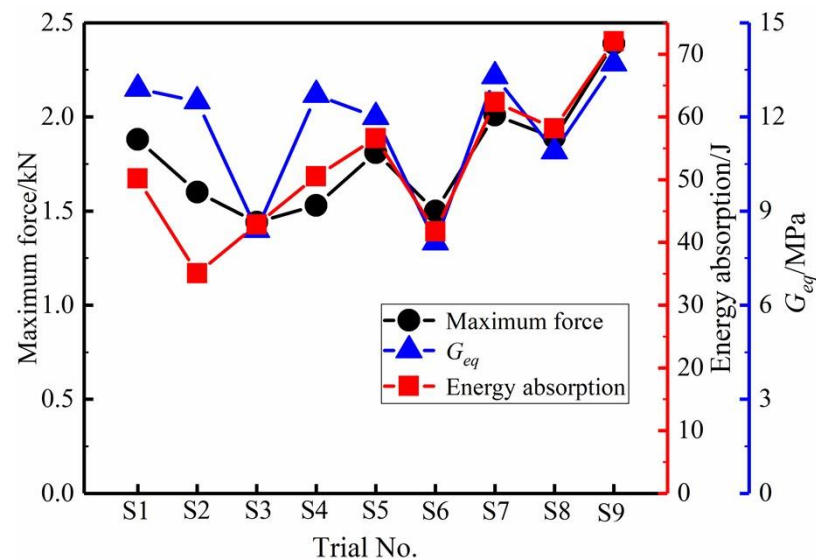
Figure 10. Evaluations of the sandwich structure on the shear properties.

The sensitivity analyses of vacuum brazing parameters on the shear properties of the sandwich structure were performed by using the software of SPSS, and the corresponding results are listed in Tables A1–A6 in Appendix A. As shown in Figure 11, the change trend between the vacuum brazing parameters and the evaluations is exhibited. Furthermore, the different vacuum brazing parameters have a similar effect on the performance of the sandwich structure. Each factor shows a similar trend in the maximum force and G_{eq}. Concerning the selected evaluations on the shear performance of the sandwich structure with different vacuum brazing parameters, the holding time is more sensitive to the shear performance than the brazing temperature and the heating rate. Therefore, the holding time is the dominant factor that affects the shear performance of the sandwich structure. The maximum force and G_{eq} of the EMWM sandwich structure exhibit first a slight decrease

and then an increase. The energy absorption has a positive correlation with the holding time. In addition, the suitable holding time for vacuum brazing is 30 min.
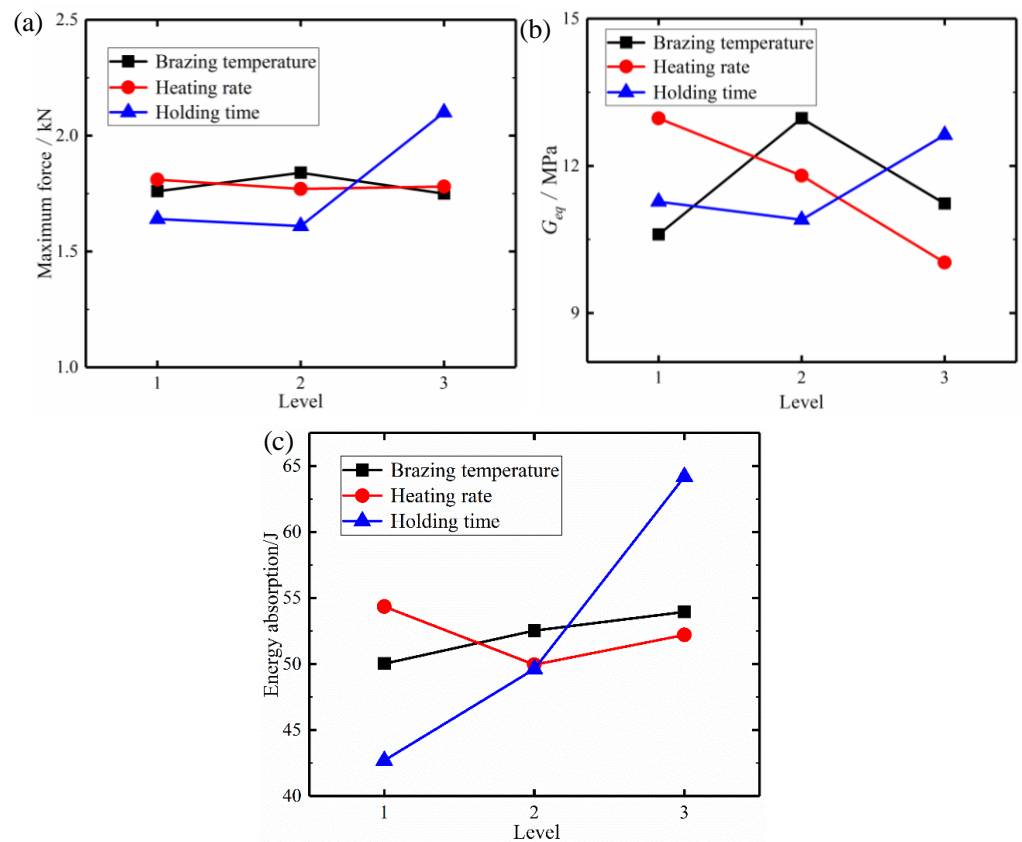
Figure 11. Relationship between vacuum brazing parameters and evaluations: (**a**) maximum force, (**b**) G_{eq}, (**c**) energy absorption.

4.3. Effect of Vacuum Brazing Parameter on the Joint Strength

The vacuum brazing process of the S3, S5, and S9 specimens were selected to fabricate a special specimen, which is composed by three-helix wires and a face-sheet. The joint strength of the wires and face-sheet is depended on the brazing process, and the specimens' failure behavior with different vacuum brazing processes can be observed by the mode-II experiment in a certain way. The failure mode of the wires and face-sheet can be divided into two modes in the mode-II experiment. Two failure behaviors (mode-I and II, as shown in Figure 12) are seen in the specimens which were fabricated by the brazing process of S3 and S5, respectively. Only one failure behavior (mode-II) is shown in the specimen with S9′s brazing parameter. At the beginning of the mode-II experiment, the helix wires were straightened and no evident failure was seen on the joint interlayer. Later, with the increase of the loading displacement, failure behavior occurred on the joint section. The wires had peeled from the face-sheet, and the obvious peeling scratches were exhibited on the face-sheet in the failure behavior of mode I. In addition, the scratches were not in a uniform line, but a curved. Owing to the special structure of the EMWM, the total connection cannot occur between the helix wires and face-sheet. However, in the mode-II failure behavior, the wires snapped and a little solder was shown in the fracture of the helix wire. Furthermore, the failure area was in the small connection area, and the reason is that the joint strength was higher than the breaking strength of the wires. Therefore, the wires snapped instead of being removed from the face-sheet when the joint strength was enough to resist the shear force.
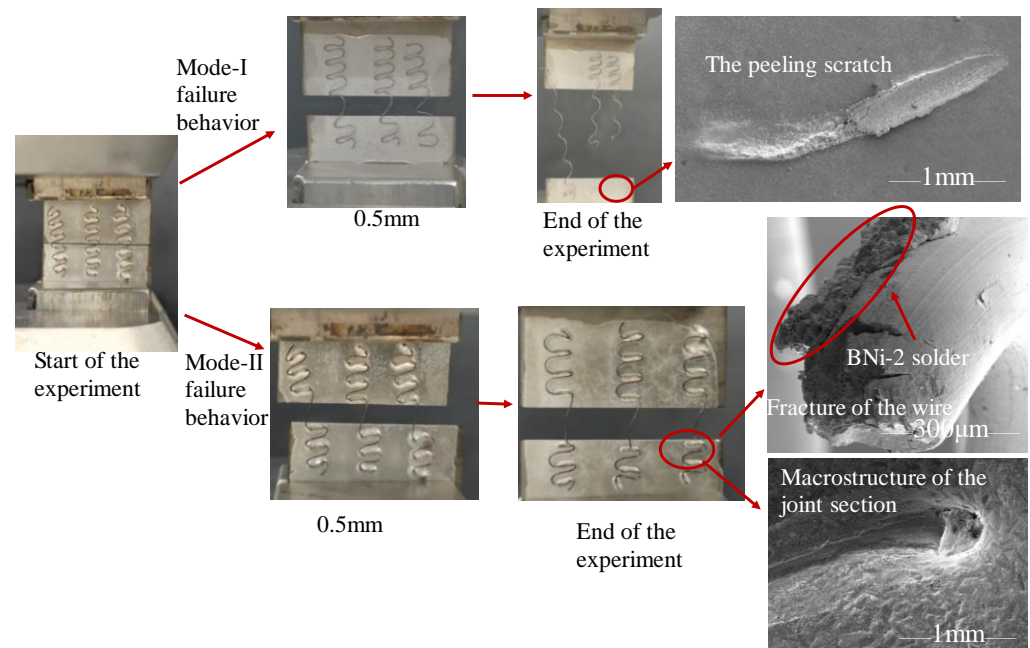
Figure 12. Failure behaviors under the mode-II experiment.

Figure 13 shows that a layer character of the EMWM material is comprised of a line and a point. Thus, the internal structure of the EMWM core has a certain indeterminacy. The joint interlayer of the EMWM sandwich structure exists in two joint states, which are line contact and point contact. Furthermore, the line contact only exists in the specimen. The complex deformation process take place among the internal helix wires in the EMWM core in the mode-I experiment. Thus, the force–displacement curves have a certain distinction and the value is disproportional to the failure behavior between the mode-II experiment and mode-I experiment.
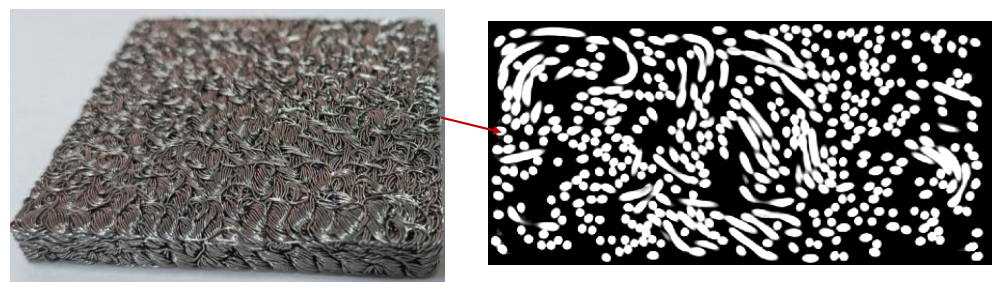
Figure 13. CT scanning photo of the EMWM core.

In Figure 14, the force–displacement curves were obtained from the mode-II experiment, and were respectively obtained from the two failure behaviors (as shown in Figure 12). The wires exhibited two different failure behaviors in the mode-II experiments. Thus, the final failure displacement of the mode-I failure behavior was longer than that of the mode-II failure behavior. As shown in Figure 14, the two failure behaviors in the mode-II experiments can be described in three stages: linear-elastic deformation stage, nonlinear elastic stage, and post-peak stage. Two failure behaviors show similar deformation during the first and second stages. However, concerning different brazed joint strengths, the peak force exhibits a large fluctuation. From Table 6, the changing trend of peak force in these three specimens increases, and the changing trend is the same as that in the sandwich structure. The peak force of the specimens is similar in the same vacuum brazing, but with different failure behavior. In the third stage, two different deformations are presented due to the different deformation of the wires. This was because they were not fractured, and were

continually being removed from the face-sheet. In the mode-I failure behavior, the force first decreases, and then increases.
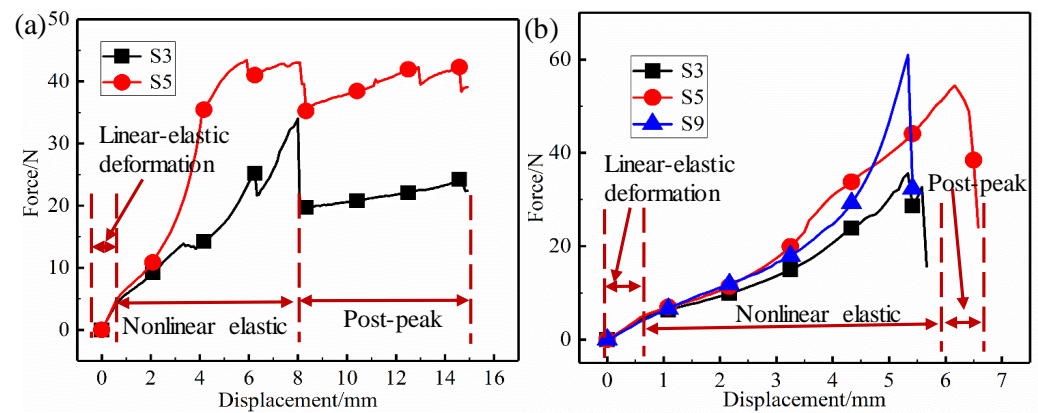
Figure 14. Force–displacement curves under the mode-II experiment: (**a**) mode-I failure behavior, (**b**) mode-II failure behavior.

Table 6. Peak force with different specimens under the mode-II experiment.

	Mode-I Failure Behavior		Mode-II Failure Behavior		
	S3	S5	S3	S5	S9
Peak force (kN)	33.97	43.03	35.58	54.39	60.98

4.4. Effect of Vacuum Brazing Parameter on the Interfacial Structure

In Figure 15, the interfacial microstructure of the elastic-porous sandwich structure can be described in five sections, i.e., the helix wire section, two diffusion layers, the BNi-2 section, and the face-sheet section. Two diffusion layers include the wire and the BNi-2 diffusion layer (D1), and the BNi-2 and face-sheet diffusion layer (D2). Figure 15 shows that the number of acicular ferrites in the S3 specimen is more than that in the S9 specimen. The acicular ferrite is a defective structure and it can cause a decrease in the mechanical performance of the joint section. Furthermore, there are obvious voids in the S3 specimen which is in the diffusion layer. The reason is that the solder diffuses insufficiently due to the low temperature and short holding time. However, the void in the S9 specimen is in the BNi-2. The reason is that the brazing temperature is too high and leads to the over-dissolution of the BNi-2 solder. Additionally, the precipitates were created in the S9 specimen. The elements Fe and Cr are from the base metal toward the solder, and the elements Ni and Fe are from the BNi-2 toward the base metal in the vacuum brazing process, as shown in Figure 16. In addition, the length of the diffusion layer is increasing in these three specimens.

Table 7 and Figure 17 show that the lengths of the diffusion layers (D1 and D2) increase in these three specimens, and the length of D1 and D2 is similar in the same specimen. Therefore, the symmetry is shown in the diffusion layers of the sandwich structure. However, the microstructure of the joint interlayer is asymmetrical, owing to the metallic wire which is the curve. In addition, the length of the diffusion layer shows that there are identical trends of the shear performance for the studied specimens. In other words, the length of the diffusion layer shows a positive correlation with the brazing joint strength and the shear performance of the sandwich structure. Therefore, the rational design of the vacuum brazing process is vital for achieving an excellent interfacial structure.
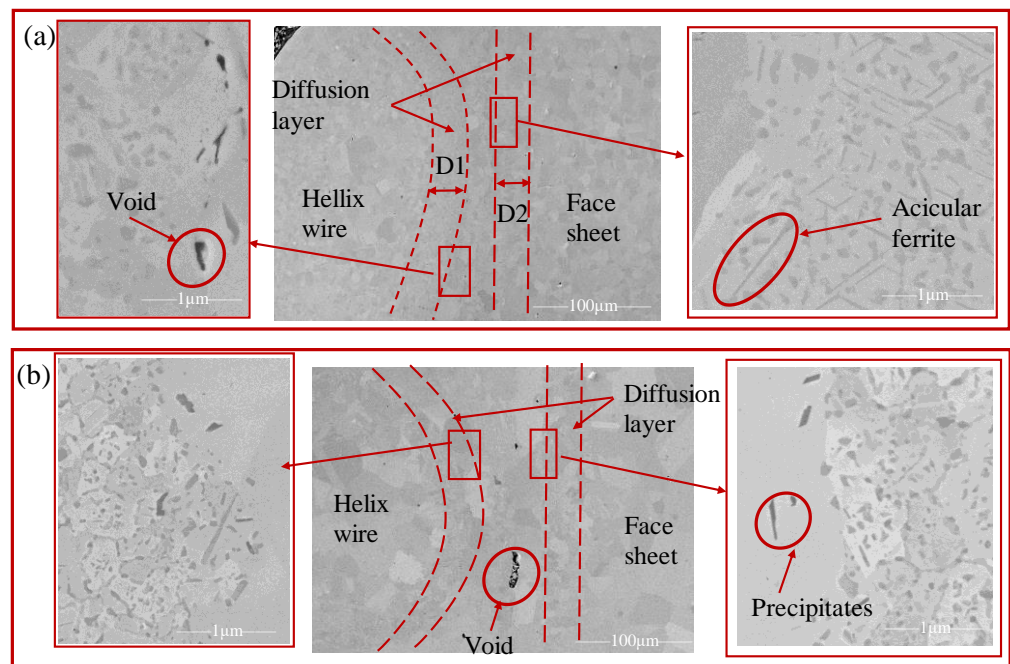
Figure 15. Interfacial structure of the sandwich structure: (**a**) S3, (**b**) S9.
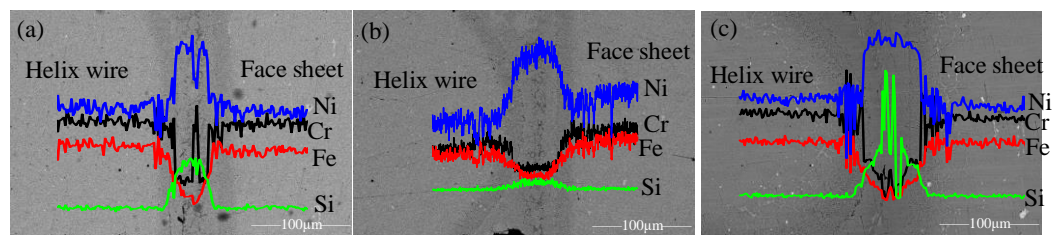
Figure 16. Line-scan analysis for distribution of the interlayer: (**a**) S3, (**b**) S5, (**c**) S9.

Table 7. Length of the diffusion layer.

Trial No.	S3		S5		S9	
	D1	D2	D1	D2	D1	D2
Length (μm)	19.97 ± 1.98	20.49 ± 2.23	26.06 ± 1.67	25.55 ± 1.70	36.25 ± 1.43	30.79 ± 2.06
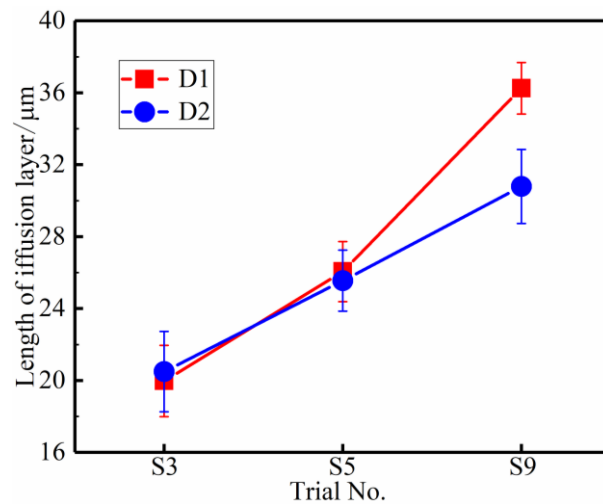
Figure 17. Length of diffusion layer in different specimens.

5. Conclusions

In order to study the effect of vacuum brazing configurations on an elastic-porous sandwich structure with the EMWM, a fabrication process and two shear experiments were performed in this work. The main conclusions that can be drawn are as follows:

(1) The typical failure behaviors of the sandwich structure involve four stages (linear, gradual-soft deformation, damage deformation, and stable damage failure) in the mode-I experiment. However, there are three stages (the linear-elastic deformation stage, nonlinear elastic stage, and post-peak stage) in the mode-II experiment. The stable damage failure stage occurs in the sandwich core of the EMWM.

(2) The failure behaviors of the sandwich structure involve the delamination failure of the EMWM core, internal friction damage of the helix wires, and peeling failure. Furthermore, the joint strength is sensitive to the vacuum brazing process, which makes a considerable effect on the interfacial microstructure and the length of the diffusion layer.

(3) Comparing with the brazing temperature and heating rate, the holding time has a huge influence on the shear performance of the sandwich structure. Moreover, the suitable holding time is about 30 min in this studied case.

Furthermore, the thermal-mechanical behavior of the sandwich structure and the control strategy by proper manufacturing technologies to avoid failure will be investigated in future work.

Appendix A

The detailed results of the orthogonal experiment design with different vacuum brazing processes by means of SPSS are presented in this section.

Table A1. Range analysis data of the peak force.

Value Name	A (Brazing Temperature (°C))	B (Heating Rate (°C/min))	C (Holding Time (min))
1	1.76	1.81	1.64
2	1.84	1.77	1.61
3	1.75	1.78	2.10
R_j	0.09	0.04	0.49

Table A2. Analysis of variance (ANOVA) of the peak force.

Source	Sum of Squares	df	Mean Squares	F Value	p
A	0.443	2	0.221	1.600	0.358
B	0.003	2	0.001	0.009	0.991
C	0.014	2	0.007	0.052	0.950
error	0.277	2	0.138	-	-

Table A3. Range analysis data of the G_{eq}.

Value Name	A (Brazing Temperature (°C))	B (Heating Rate (°C/min))	C (Holding Time (min))
1	10.60	12.97	11.27
2	12.97	11.80	10.90
3	11.23	10.03	12.63
R_j	2.37	2.94	1.73

Table A4. Analysis of variance (ANOVA) of the G_{eq}.

Source	Sum of Squares	d_f	Mean Squares	F Value	p
A	5.007	2	2.503	0.645	0.608
B	13.087	2	6.543	1.686	0.372
C	9.007	2	4.503	1.161	0.463
error	7.760	2	3.880	-	-

Table A5. Range analysis data of the energy absorption.

Value Name	A (Brazing Temperature (°C))	B (Heating Rate (°C/min))	C (Holding Time (min))
1	50.03	54.36	42.69
2	52.53	49.95	49.62
3	53.95	52.20	64.19
R_j	3.92	4.41	21.57

Table A6. Analysis of variance (ANOVA) of the energy absorption.

Source	Sum of Squares	d_f	Mean Squares	F Value	p
A	722.662	2	361.331	2.633	0.275
B	29.220	2	14.610	0.106	0.904
C	23.640	2	11.820	0.086	0.921
error	274.420	2	137.210	-	-

References

1. Xiong, J.; Ma, L.; Pan, S.; Wu, L.; Papadopoulos, J.; Vaziri, A. Shear and bending performance of carbon fiber composite sandwich panels with pyramidal truss cores. *Acta. Mater.* **2012**, *60*, 1455–1466. [CrossRef]
2. Liviu, M.; Ffilippo, B.; Dan, A.S.; Bai, H.B.; Emanoil, L. An engineering approach to predict mixed mode fracture of PUR foams based on ASED and micromechanical modelling. *Theor. Appl. Fract. Mech.* **2017**, *91*, 148–154.
3. Funari, M.F.; Spadea, S.; Lonetti, P.; Lourenço, P.B. On the elastic and mixed-mode fracture properties of PVC foam. *Theor. Appl. Fract. Mech.* **2021**, *112*, 102924. [CrossRef]
4. Mostafa, A.; Shankar, K.; Morozov, E.V. Insight into the shear bahaviour of composite sandwich panels with foam core. *Mater. Des.* **2013**, *50*, 92–101. [CrossRef]
5. Liu, Y.; Liu, W.; Gao, W.C. Out-of-plane shear property analysis of Nomex honeycomb sandwich structure. *J. Reinf. Plast. Compos.* **2021**, *40*, 165–175. [CrossRef]
6. Huang, W.; Fan, Z.H.; Zhang, W.; Liu, J.Y.; Zhou, W. Impulsive response of composite sandwich structure with tetrahedral truss core. *Compos. Sci. Technol.* **2019**, *176*, 17–28. [CrossRef]

7.   Mei, J.; Ao, Y.L.; Jiang, W.M.; Liu, J.Y.; Zhou, G.; Huang, W. Investigation on the shear behaviors of carbon fiber composite sandwich panels with the X-core. *Mater. Struct.* **2021**, *77*, 102897. [CrossRef]

8.   Zhang, P.; Cheng, Y.S.; Liu, J.; Wang, C.M.; Hou, H.L.; Li, Y. Experimental and numerical investigations on laser-welded corrugated-core sandwich panels subjected to air blast loading. *Mar. Struct.* **2015**, *40*, 225–246. [CrossRef]

9.   Yang, P.; Bai, H.B.; Xue, X.; Xiao, K.; Zhao, X. Vibration reliability characterization and damping capability of annular periodic metal rubber in the non-molding direction. *Mech. Syst. Signal Proc.* **2019**, *132*, 622–639. [CrossRef]

10. Xue, X.; Ruan, S.X.; Bai, H.B.; Chen, X.C.; Shao, Y.C.; Lu, C.H. An enhanced constitutive model for the nonlinear mechanical behavior of the elastic-porous metal rubber. *Mech. Mater.* **2020**, *148*, 103447. [CrossRef]

11. Wang, Y.J.; Zhang, Z.J.; Xue, X.M.; Zhang, L. Experimental investigation on enhanced mechanical and damping performance of corrugated structure with metal rubber. *Thin-Walled Struct.* **2020**, *154*, 106816. [CrossRef]

12. Yan, H.B.; Mew, T.; Lee, M.G.; Kang, K.J.; Lu, T.J.; Kienhöfer, F.W.; Kim, T. Thermofluidic characteristics of a porous ventilated brake disk. *J. Heat Transf.-Trans. ASME* **2015**, *137*, 022601. [CrossRef]

13. New, T.D.; Kang, K.; Kienhöfer, F.W.; Kim, T. Transient thermal response of a highly porous ventilated brake disc. *Proc. Inst. Mech. Part D-J. Automob. Eng.* **2015**, *229*, 674–683.

14. Zhu, Y.; Wu, Y.W.; Bai, H.B.; Ding, Z.Y.; Shao, Y.C. Research on vibration reduction of foundation with entangled metallic wire material under high temperature. *Shock Vib.* **2019**, *2019*, 7297392. [CrossRef]

15. Nanayakkara, A.M.; Feih, S.; Mouritz, A.P. Improving the fracture resistance of sandwich composite T-joints by z-pinning. *Compos. Struct.* **2013**, *96*, 207–215. [CrossRef]

16. Gao, F.; Wang, L.F.; Hua, J.D.; Lin, J.; Mal, A. Application of Lamb wave and its coda waves to disbond detection in an aeronautical honeycomb composite sandwich. *Mech. Syst. Signal Proc.* **2021**, *146*, 107063. [CrossRef]

17. Peng, F.H.; Wu, Y.W.; Bai, H.B.; Shao, Y.C.; Qin, Z.Q. Influence of core thickness and boundary condition on the modal characteristics of composite structure with metallic damping core. *Shock Vib.* **2020**, *2020*, 9720167. [CrossRef]

18. Lin, C.; Lee, F.C.; Xue, T.H. Effect of suture on mechanical properties of stitched thermal protection sandwich. *Mater. Res.-Ibero-Am. J. Mater.* **2019**, *22*, e20190435. [CrossRef]

19. Yudhanto, A.; Watanabe, N.; Iwahori, Y.; Hoshi, H. Effect of stitch density on tensile properties and damage mechanisms of stitched carbon/epoxy composites. *Compos. Pt. B-Eng.* **2013**, *46*, 151–165. [CrossRef]

20. Wang, S.S.; Wei, Y.H.; Xue, X.; Wu, Z.B.; Bai, H.B. Connection technology and mechanical properties of sandwich structure with the core of elastic damping metal spiral wire mesh. *Acta Mater. Compos. Sin.* **2022**, *39*, 1308–1321.

21. Srinivasan, G.; Bhaduri, A.K.; Ray, S.K.; Shankar, V. Vacuum brazing of Inconel 600 sleeve to 316L stainless steel sheath of mineral insulated cable. *J. Mater. Process. Technol.* **2008**, *198*, 73–76. [CrossRef]

22. Hebda, M.; Kaczor, P.; Miernik, K. Vacuum brazing of stainless steel depending on the surface preparation method and temperature of the process. *Arch. Metal. Mater.* **2019**, *64*, 5–11.

23. Ivannikov, A.; Krasnova, E.; Penyaz, M.; Popov, N.; Melnikov, A.; Sevryukov, O. Effect of high-temperature brazing with a nickel-based STEMET 1301A brazing alloy on the unbrazing temperature of 12Kh18N10T steel joints. *Int. J. Adv. Manuf. Technol.* **2020**, *110*, 1319–1326. [CrossRef]

24. Chen, Y.X.; Cui, H.C. Effect of temperature and hold time of induction brazing on microstructure and shear strength of martensitic stainless steel joints. *Materials* **2018**, *11*, 1586. [CrossRef]

25. Liu, S.L.; Miao, J.K.; Zhang, W.W.; Wei, R.; Chen, C.; Wang, T.; Zhao, W.D. Interfacial microstructure and shear strength of TC4 alloy joints vacuum brazed with Ti–Zr–Ni–Cu filler metal. *Mater. Sci. Eng. A-Struct. Mater. Prop. Microstruct. Process.* **2020**, *775*, 138990. [CrossRef]

26. Zaharinie, T.; Yusof, F.; Hamdi, M.; Ariga, T.; Moshwan, R. Effect of brazing temperature on the shear strength of Inconel 600 joint. *Int. J. Adv. Manuf. Technol.* **2014**, *73*, 1133–1140. [CrossRef]

27. Chakraborty, G.; Chaurasia, P.K.; Murugesan, S.; Albert, S.K.; Murugan, S. Effect of brazing temperature on the microstructure of martensitic-austenitic steel joints. *Mater. Sci. Technol.* **2017**, *33*, 1372–1378. [CrossRef]

28. Jiang, W.C.; Gong, J.M.; Tu, S.T. Effect of holding time on vacuum brazing for a stainless steel plate–fin structure. *Mater. Des.* **2010**, *31*, 2157–2162. [CrossRef]

29. Jiang, W.C.; Gong, J.M.; Tu, S.T. A new cooling method for vacuum brazing of a stainless steel plate–fin structure. *Mater. Des.* **2010**, *31*, 648–653. [CrossRef]

30. Sohrabi, M.J.; Mirzadeh, H.; Rafiei, M. Solidification behavior and Laves phase dissolution during homogenization heat treatment of Inconel 718 superalloy. *Vacuum* **2018**, *154*, 235–243. [CrossRef]

31. Courtois, L.; Maire, E.; Perez, M.; Rodney, D.; Bouaziz, O.; Brechet, Y. Mechanical properties of monofilament entangled materials. *Adv. Eng. Mater.* **2012**, *14*, 1128–1133. [CrossRef]

32. Hu, J.L.; Du, Q.; Gao, J.H.; Kang, J.Y.; Guo, B.T. Compressive mechanical behavior of multiple wire metal rubber. *Mater. Des.* **2018**, *140*, 231–240. [CrossRef]

33. Zhang, W.; Xue, X.; Bai, H.B. Mechanical and electrical properties of Cu-steel bimetallic porous composite with a double-helix entangled structure. *Compos. Struct.* **2021**, *255*, 112886. [CrossRef]

34. Ma, Y.H.; Zhang, Q.C.; Zhang, D.Y.; Scarpa, F.; Liu, B.L.; Hong, J. Turning the vibration of a rotor with shape memory alloy metal rubber supports. *J. Sound. Vib.* **2015**, *351*, 1–16. [CrossRef]

35. Zhang, D.Y.; Scrapa, F.; Ma, Y.H.; Boba, K.; Hong, J.; Lu, H.W. Compression mechanics of nickel-based superalloy metal rubber. *Mater. Sci. Eng. A-Strut. Prop. Microstruct. Process.* **2013**, *580*, 305–312. [CrossRef]
36. Xue, X.; Yang, P.; Shao, Y.C.; Bai, H.B. Manufacture technology and anisotropic behaviour of elastic-porous metal rubber. *Int. J. Lightweight Mater. Manuf.* **2020**, *3*, 88–99. [CrossRef]
37. Arcieri, E.V.; Baragetti, S.; Božić, Z. Application of design of experiments to foreign object damage on 7075-T6. *Procedia Struct. Integr.* **2021**, *31*, 22–27. [CrossRef]
38. Lloyd, W.C. *Reliability Improvement with Design of Experiments*, 2nd ed.; CRC Press: Boca Raton, FL, USA, 1991; pp. 30–140.